Journal of Hazardous Materials 400 (2020) 123186

Contents lists available at ScienceDirect

Journal of Hazardous Materials

journal homepage: www.elsevier.com/locate/jhazmat

# Comprehensive characterization and environmental risk assessment of end-of-life automotive catalytic converters to arrange a sustainable roadmap for future recycling practices

Nazanin Bahaloo-Horeh, Seyyed Mohammad Mousavi*

*Biotechnology Group, Chemical Engineering Department, Tarbiat Modares University, Tehran, Iran*

## GRAPHICAL ABSTRACT

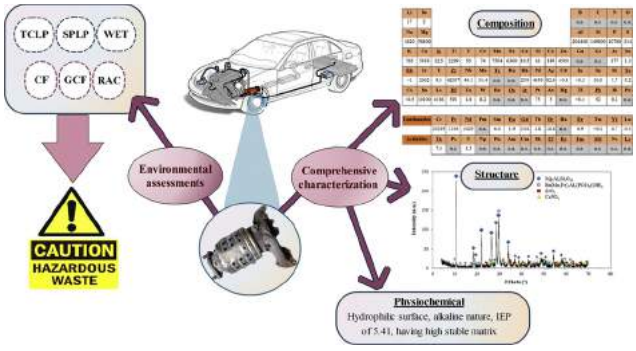


## ARTICLE INFO

Editor: Daniel CW Tsang

*Keywords:*
Heavy metals
Characterization analyses
Sequential extraction
Toxicity tests
Contamination index

## ABSTRACT

Environmentally appropriate economic recycling of spent automotive catalytic converters (SACCs) is difficult due to their complexity. The prominent reason is the lack of knowledge and comprehensive characterization of SACCs. This study focused on the characterization of SACCs in terms of their structural, morphological, physiochemical, surface, and thermal properties. The accurate determination of metals content, including 4975 mg/kg platinum group metals, 42,119 mg/kg rare earth elements, and other base metals, showed a great potential wealth in SACCs. Besides, the sequential extraction method was applied for metals fractionation, which represents a unique harsh recycling approach needed due to the stable structure of SACCs, metals embedded in silicate phases, and the presence of barely soluble metal phosphates. This waste was also examined for environmental criteria and leaching tests, including Toxicity Characteristic Leaching Procedure, Waste Extraction Test, and Synthetic Precipitation Leaching Procedure. The findings declare that Waste Extraction Test was the

*Abbreviations:* ANC, Acid neutralization capacity; BCR, Bureau of Community Reference; BET, Brunauer–Emmett–Teller; BJH, Barrett-Joyner-Halenda; BSE, Backscattered electron detector; CDTSC, California Department of Toxic Substances Control; CF, Contamination factor; EDX, Energy dispersive X-ray spectroscopy; FCC-SC, Fluidized catalytic cracking-spent catalyst; FESEM, Field emission scanning electron microscopy; FTIR, Fourier transforms infrared spectroscopy; GCF, Global contamination factor; ICP-MS, Inductively coupled plasma- mass spectrometry; IEP, Isoelectric point; LCD, Liquid crystal display; LED, Light emitting diode; LIB, Lithium ion battery; MSWI, Municipal solid waste incineration; PGM, Platinum group metal; PCB, Printed circuit board; PSA, Particle size analyzer; PZC, Point of zero charge; RAC, Risk assessment code; REE, Rare earth element; SACC, Spent automotive catalytic converter; SE, Secondary electron detector; SPLP, Synthetic precipitation leaching procedure; STP, Standard temperature and pressure; TCLP, Toxicity characteristic leaching procedure; TGA-DTA, Thermal gravimetric analyzer-differential thermal analyzer; USEPA, United States Environmental Protection Agency; WET, Waste extraction test; XRD, X-ray diffraction spectrometry; XRF, X-ray fluorescence spectrometry

* Corresponding author at: P.O. Box: 14115-111, Jalal Ale Ahmad Highway, Tarbiat Modares University, Tehran, Iran.
*E-mail address:* mousavi_m@modares.ac.ir (S.M. Mousavi).

https://doi.org/10.1016/j.jhazmat.2020.123186
Received 10 March 2020; Received in revised form 1 June 2020; Accepted 8 June 2020
Available online 15 June 2020

most aggressive procedure to assess mobility. The contamination indexes, such as risk assessment code, contamination factor, and global contamination factor, were also investigated, which show SACCs must be regarded as hazardous waste. As an example, the global contamination factor of 11.87 depicts SACCs have a moderate contamination degree.

## 1. Introduction

Modern cars are outfitted with catalytic converters that convert toxic compounds of exhaust gas, such as $NO_x$, unburned $C_xH_y$, and CO, into non-toxic $N_2$, $H_2O$, and $CO_2$ (Karim and Ting, 2020). Automotive catalysts' activity is reduced with time due to the deposition of contaminants or the sintering process in high operating temperatures. When regeneration of automotive catalysts is no longer an appropriate choice, they are considered solid waste (Firmansyah et al., 2019; Zhao et al., 2019a).

The global annual sales of catalytic converter rose from over 9 million units in 2006 to around 19 million units in 2012, and it was around 140 million units by 2019 (Islam et al., 2018). Besides, the stock of spent automotive catalytic converters (SACCs) increases steadily with the increasing number of cars in the world (Morcali, 2020). It has estimated that the vehicle count increases close to 2 billion by the year 2030 (Malhotra et al., 2015). The increase in the production and consumption of catalytic converters has augmented the amount of SACCs. Consequently, a considerable amount of SACCs is disposed of and accumulated in landfills and scrap disposal sites (Choi et al., 2018).

With the inappropriate disposal of SACCs, the heavy metals presented in them can be released into the atmosphere, water, and soil, which ultimately causes the transfer of metals to the food chain (Bahaloo-Horeh et al., 2019). It was shown that the probability of metals absorption by the human body from the food and environment is increasing, which leads to the formation of different diseases (Wang et al., 2017). The harmful effects of some metals presented in SACCs are as follows: platinum group metals (PGMs) can cause respiratory sensitization, allergic reactions, dermatitis, lymphocyte proliferation, and cytokine release and possibly to cancer (Kalavrouziotis and Koukoulakis, 2009; Senthil et al., 2017); Al has adverse effects on the nervous system and resulted in Alzheimer disease, problems with balance and coordination loss (Jaishankar et al., 2014); rare earth elements (REEs) cause renal fibrosis, peritoneal adhesion, bloody ascites, disseminated peritonitis, opacification, and swelling of the liver (Wang et al., 2017).

The waste management options rely mostly on whether a waste is hazardous or not. Recently, various leaching tests, such as toxicity characteristic leaching procedure (TCLP), synthetic precipitation leaching procedure (SPLP), waste extraction test (WET), and acid neutralization capacity (ANC), were applied to evaluate the metals leachability, simulate the rainfall or landfill conditions, and determine whether a waste is potentially hazardous or not (Hira et al., 2018). These leaching tests were performed on different waste, such as liquid crystal display (LCD) (Yeom et al., 2018), light emitting diode (LED) lamps (Kumar et al., 2019), fluidized catalytic cracking-spent catalysts (FCC-SCs) (Azevedo et al., 2019), municipal solid waste incineration (MSWI) fly ash (Funari et al., 2017), electroplating sludge (Nikfar et al., 2020), lithium ion batteries (LIBs) (Winslow et al., 2018), printed circuit boards (PCBs) (Priya and Hait, 2019), mobile phones (Hira et al., 2018; Chen et al., 2018), and alkaline button-cell batteries (Sadeghabad et al., 2019), which showed these waste require treatment before disposal and should be considered as hazardous. However, the hazard of SACCs under different environmental conditions has not been regarded up to now.

On the other hand, the determination of metals fractionation in the SACCs matrix could provide detailed information about leaching behavior, bioavailabilities, and environmental risks (Gwebu et al., 2017). Different studies attempted to define the metals fractionation in solid matrices. However, the obtained results of these studies were not comparable due to the use of different procedures, varying in the number of steps, types of reagent, and extraction conditions (de Andrade Passos et al., 2010). To standardize the various fractionation approaches reported within the literature, a modified sequential extraction procedure was recommended by the European Bureau of Community Reference (BCR) (Macías et al. (2017)). According to the BCR protocol, metals are fractionated into acid-soluble, reducible, oxidizable, and residual forms (Dai et al., 2018). Despite the usefulness of this procedure, there is no information yet on the metals fractionation of SACCs.

However, recycling is the most effective way for waste management. The high metal content in SACCs and a significant volume of generating SACCs could make a sustainable reverse supply chain of metals for the industry and give this waste real market value. For further clarity, it should be said that nowadays, 98 % of the automobiles have catalytic converters, which show how large the volume of waste is produced (Rzelewska and Regel-Rosocka, 2018). In the case of PGMs, the manufacturing of automotive converters consumes 80 % of total world production of Pd, 80 % of Rh, and 50 % of Pt (Karim and Ting, 2020). It is worth noting that 1 kg of Pt can be obtained by processing 2 tons of SACCs or by outputting 150 tons of ore, which shows SACCs have very rich metal content (Fornalczyk and Saternus, 2013).

There are different approaches for metal recovery from SACCs according to techniques of pyrometallurgy (Chen et al., 2015; Spooren and Atia, 2020), hydrometallurgy (Firmansyah et al., 2019), and biohydrometallurgy (Karim and Ting, 2020). The design of processes for metals recovery from SACCs with favorable efficiency and performance needs a complete understanding of the SACCs characteristics (Fontana et al., 2019). Due to the complexity of the waste matrix, characterization analyses provide insights for actors involved in material sustainability and recycling processes. Previous works attempted to characterize various waste, including LED lamps (Rebello et al., 2020), mobile phones (Fontana et al., 2019; Singh et al., 2018), Zn-$MnO_2$ batteries (Cabral et al., 2013), and desktop computers (Kohl and Gomes, 2018), which showed comprehensive characterization could be used as a tool for establishing a knowledge base for new recycling approaches. However, the comprehensive characterization of SACCs has not been sufficiently explored to arrange a sustainable roadmap for recycling and managing SACCs; hence study in this area is essential.

With these points in mind, we tried to fulfill the mentioned gaps in this research. Briefly, the objectives of this paper are (1) comprehensive characterization of the SACCs to provide helpful details for future recycling practices; (2) to investigate the metals fractionation of SACCs using modified BCR procedure; (3) to assess the metals contamination degree with the aid of risk assessment code (RAC), contamination factor (CF), and global contamination factor (GCF); (4) to provide quantitative data for leachable metals concentration from SACCs under simulated conditions of acid rain and landfills according to the ANC, TCLP, WET, and SPLP; (5) to investigate the total economic value of metals contained in SACC.

## 2. Materials and methods

### 2.1. Preparation of SACCs powder

For the characterization of the SACCs, the first step is to collect the catalytic converters. The PGM-containing SACCs used in this work were collected from the automobile service and repair shops. The collected

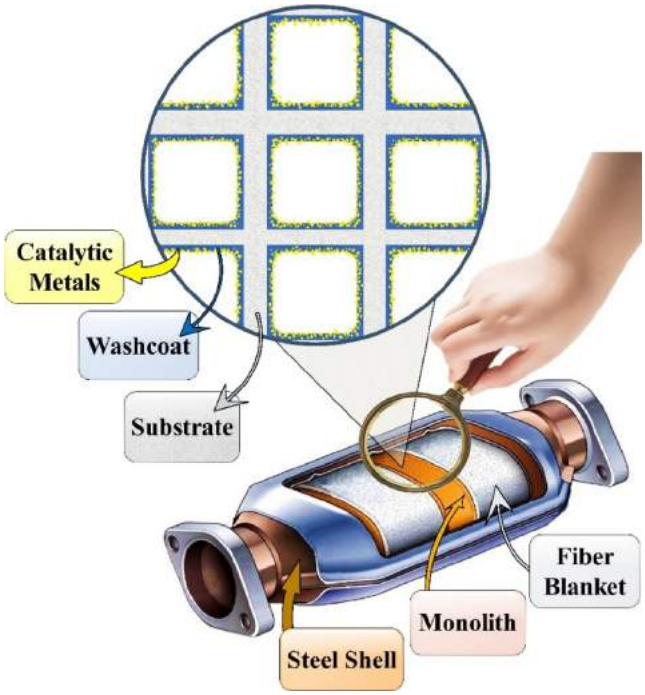


**Fig. 1.** Different parts of the automotive catalytic converter.

SACCs were made from the same manufacturer and contain a ceramic carrier. The second step is the mechanical dismantling of SACCs. However, it is essential to know about the structure of catalytic converters to carry out proper dismantling. Fig. 1 depicts different fragments of the catalytic converter, including monolith, the outer steel shell, and the fiber blanket. The honeycomb monolith typically consists of a synthetic skeleton, which is made of ceramic as cordierite and zeolite or metallic carrier. This skeleton is coated with a washcoat layer, which is made of a mixture of $\gamma$–$Al_2O_3$ and base metal oxides. The catalytic substances (PGMs) are dispersed on the washcoat layer by coating or impregnation from Pt, Pd, and Rh chloro-complexes solution (Voncken, 2019).

For dismantling SACCs, they were carefully opened by slicing the steel shell through a grinding machine to extract the ceramic honeycomb monolith, which surrounded by a fiber blanket. Next, the fibrous wrapping was removed. The honeycomb structure monolith was crushed with a hammer, followed by a milling process via a ball mill. Subsequently, it was sieved to achieve a powder with a particle size of less than 75 μm to facilitate subsequent characterizations. Finally, the powdery sample, which exhibited a gray appearance, was dried at 100 °C to obtain accurate results. All experiments were conducted on samples taken from the prepared powder. The flowsheet of powder preparation is illustrated in Fig. 2.

### 2.2. Waste characterization analyses

The concentrations of metals in the SACCs powder were determined by using both inductively coupled plasma-mass spectrometry (ICP-MS) after the digestion process and X-ray fluorescence spectrometry (XRF; PW2404, Philips, Netherlands) analysis. Sulfur, nitrogen, hydrogen, and carbon contents of SACCs powder were determined using a CHNS Elemental Analyzer (ECS 4010, Costech, Italy). The details of the chemical digestion procedure and CHNS analysis are reported in supporting information.

X-ray diffraction spectrometry (XRD; Bruker AXS D8 Advance, Germany) was performed to identify the phase constitutions of the SACCs powder and analyze its crystalline structure. The conditions included Cu Kα radiation, current: 30 mA, accelerating voltage: 40 kV, range: $4^\circ \leq 2\theta \leq 70^\circ$, step: 0.02°/s. To study the functional groups in the SACCs powder, Fourier transforms infrared spectroscopy (FTIR; Frontier, Perkin-Elmer, USA) was used at a frequency range of 400–4000 $cm^{-1}$. The morphology and distribution of the main elements of SACCs were analyzed by field emission scanning electron microscopy (FESEM; MIRA3 TESCAN-XMU, Czech Republic) through a secondary electron (SE) and backscattered electron (BSE) detectors equipped with an energy dispersive X-ray spectroscopy (EDX) detector.

The changes in the mass of the SACCs powder over time as a function of temperature were analyzed using a thermal gravimetric analyzer-differential thermal analyzer (TGA-DTA; Mettler Toledo, Switzerland). In this line, 20 mg of SACCs powder was heated from 25 to 1200 °C in an air atmosphere with an airflow of 50 mL/min and a heating rate of 10 °C/min.

A particle size analyzer (PSA; Sympatec GmbH, Clausthal-Zellerfeld, Germany) was applied for analyzing the particle size distribution of SACCs powder. To investigate the surface area, pore volume, and the pore size of the powder, the Brunauer–Emmett–Teller (BET) analysis, which uses nitrogen adsorption-desorption, could be employed (Xiang et al., 2020). The details of BET analysis are reported in supporting information.

The real density of SACCs powder was determined with a pycnometer based on ISO 17,892-part 3 (2015) at 25 °C and humidity of 30 % (ISO17892-part3, 2015). The water contact angle of SACCs powder was carried out using the sessile drop method with a Dataphysics OCA-20 contact angle analyzer (Dataphysics Inc., GmbH, Germany). The initial pH of SACCs powder was defined by adding 1 g of powder in 50 mL of deionized water and shaking at 30 °C for 24 h and 160 rpm (Naseri et al., 2019). Then, the pH of the mixture was measured by a digital multimeter (CP-500 L, ISTEK, South Korea).

The point of zero charges (PZC) or isoelectric point (IEP) is a point at which the zeta potential is zero in the particular pH. In this regard, electrophoretic mobility of SACCs powder was measured at different pH conditions through the zeta potential analyzer (Particle Metrix, Meerbusch, Germany) to determine the IEP of the SACCs powder. The details of IEP determine are reported in supporting information.

### 2.3. Environmental assessments

#### 2.3.1. Metals fractionation

The modified BCR sequential extraction procedure was performed on SACCs powder to determine its metals fractionation. Comprehensive information on the modified BCR protocol is described below (Gwebu et al., 2017; Macías et al., 2017; Dai et al., 2018; Gao et al., 2018; Mittermüller et al., 2016):

*First step (Fraction 1):* 1 g of SACCs powder was added to 40 mL of 0.11 M acetic acid solution, and the mix was agitated for 16 h at 22 °C. The mix was centrifuged for 20 min; then, the supernatant was filtered and analyzed for metals concentration. Before performing the next extraction step, the remaining solid was washed with deionized water (20 mL) by agitating for 15 min and afterward centrifuged for 20 min; this supernatant discarded. The metals extracted in this stage are related to weak acid-soluble fraction and metals that are exchangeable, weakly adsorbed, have loosely bound or associated with carbonates. The presented metals in this stage would be released if environmental conditions turned into slightly acidic.

*Second step (Fraction 2):* The residue from the previous step was added to 40 mL of a 0.5 M freshly prepared hydroxylammonium chloride solution, which acidified by the addition of 2 M $HNO_3$ solution to pH around 1.5. Again, the mixture was shaken at 22 °C for 16 h. The separation of extract from the solid residue and then washing the residue were performed as described in the first step. Metals extracted in this stage are related to easily reducible fractions and metals that are associated with oxides of Fe and Mn, which would be released if the oxic state of solid sample changes to an anoxic state (or the sample exposed to more reductive conditions). Generally, when the oxides of

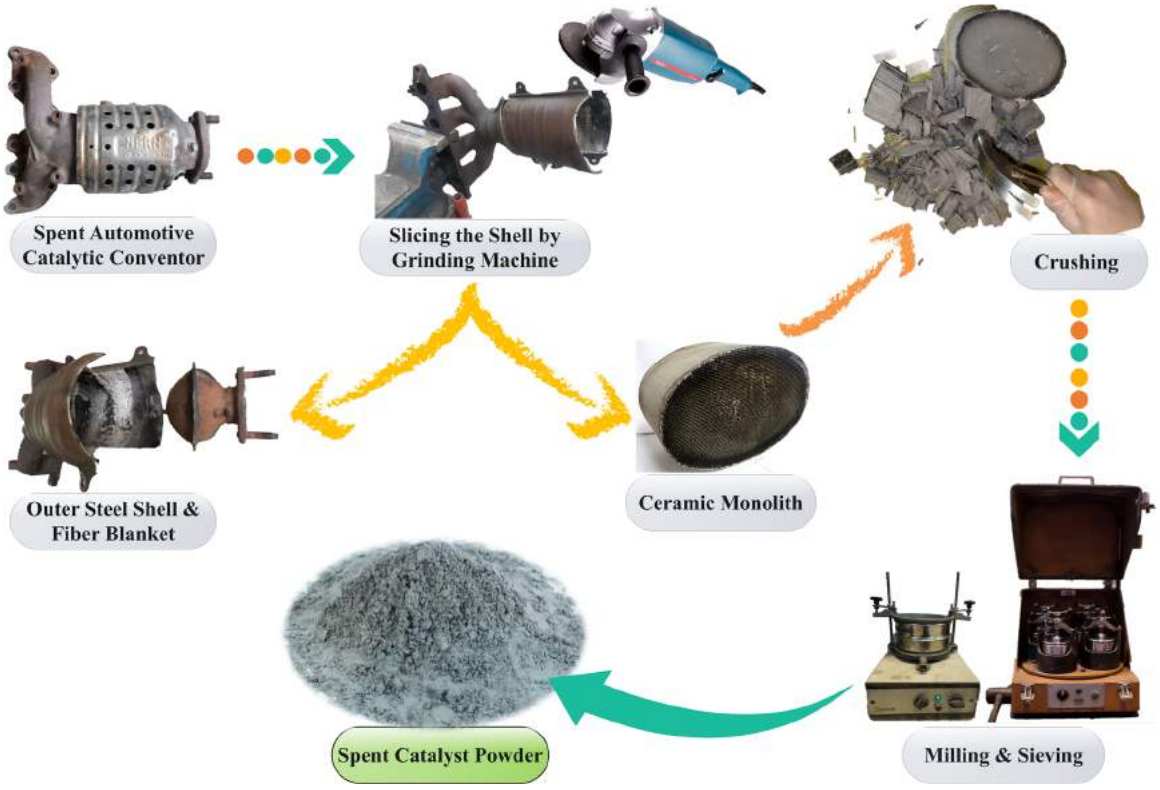


**Fig. 2.** Flowsheet of the SACCs powder preparation procedure.

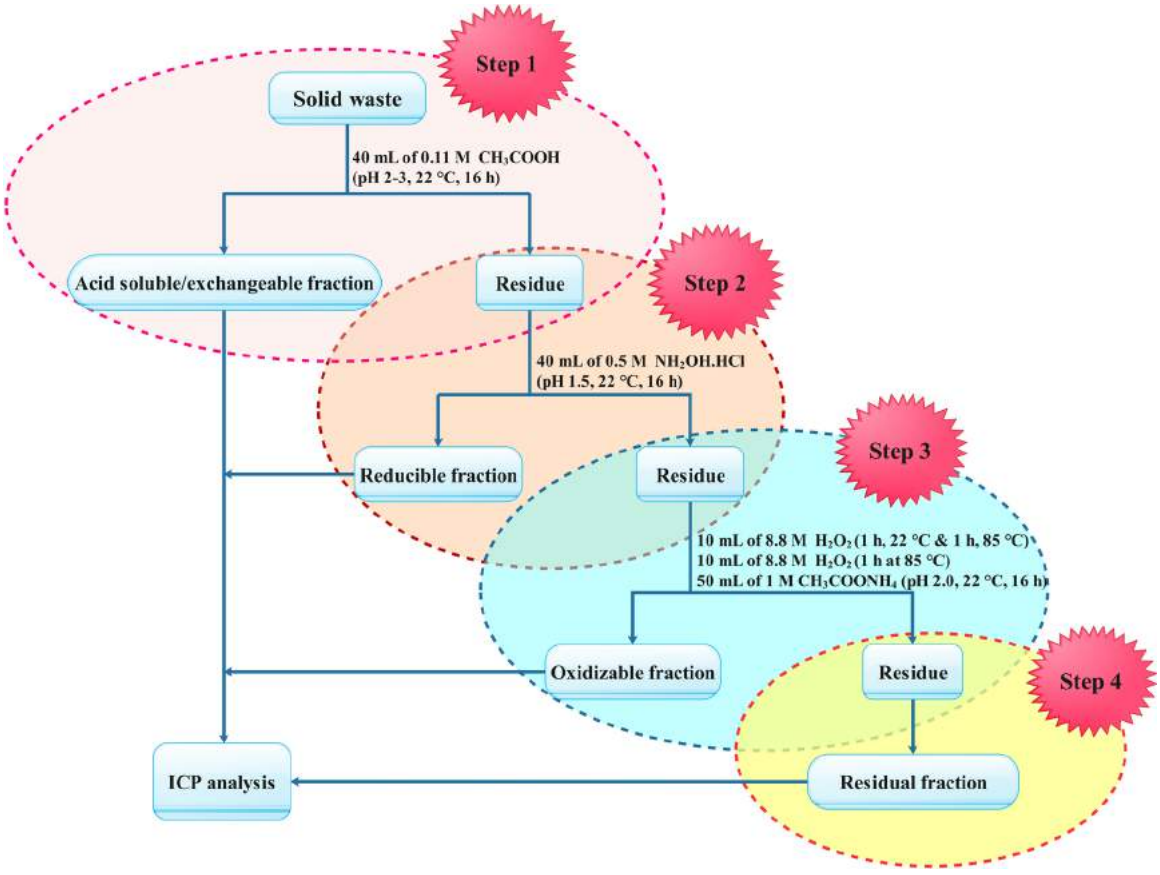


**Fig. 3.** A schematic diagram of the BCR procedure.

Fe and Mn, which are excellent trace metals scavengers, go through anoxic conditions, they become thermodynamically unstable. If Eh and pH of reagents were controlled, all or some of the metal oxides could be dissolved.

*Third step (Fraction 3):* The residue from the previous step was added to 10 mL of 8.8 M hydrogen peroxide solution (pH 2–3). The mixture of solid residue and $H_2O_2$ left for 1 h at room temperature. Then, the mixture was digested in a water bath for 1 h at 85 °C until the mix's volume was decreased to 2 − 3 mL. A second 10 mL of 8.8 M $H_2O_2$ solution was added, and then again digested for 1 h at a temperature of 85 °C, until the volume evaporated to near dryness. Finally, after cooling down to room temperature, 50 mL of 1 M ammonium acetate solution, which was acidified to pH 2 by the addition of concentrated $HNO_3$ solution, was added to the residue and shaken at 22 °C for 16 h. As in previous steps, the separation of extract from the solid residue and then washing the solid residue were performed. The metals extracted at this stage are related to oxidizable fractions and metals associated with sulfides and organic matter. The presented metals in this stage need highly oxidizing environmental conditions to be released from the matrix.

*Fourth step (Fraction 4):* The metals concentration of solid residue at the end of the BCR procedure could be determined by calculating the concentration of the remaining metals after the above three steps (the difference between the total metal concentration of solid residue and the sum of the metal concentration in three above fractions). The metals extracted in this stage are related to residual fraction and metals that are attributed to the crystalline matrix. These metals could not be released under normal environmental conditions.

A schematic diagram of the described BCR procedure is represented in Fig. 3. In all the experiments, the extraction recovery is defined as the following equation:

$$\text{Metal recovery} = \frac{C_S \times V_S}{C_T \times M_T} \times 100\,\% \quad (1)$$

where $C_S$ is elemental content in leach liquor (mg/L), $C_T$ is the elemental content in SACCs (mg/g), $V_S$ is the leaching solution volume (L), and $M_T$ is the SACCs mass (g).

*2.3.1.1. Environmental implications*. The CF, GCF, and RAC are tools criteria for investigating the relative metals retention time, which implies the environmental risk degree of metals. Table 1 shows the CF, GCF, and RAC calculation (ELTurk et al., 2018; Soliman et al., 2018; Zhao et al., 2019b).

### 2.3.2. TCLP, WET, and SPLP tests

For determining the hazard of waste, several approaches such as TCLP, WET, and SPLP have been suggested by environmental agencies at the international, national, and state levels. If the concentration of leached metals from waste surpasses the threshold limits, the waste is categorized as a hazardous substance (Hira et al., 2018). It should be noted that TCLP and WET simulate the conditions for the metals leachability from waste disposed inside landfills. Besides, SPLP demonstrates the effect of rainfall on the mobility of metals from waste (Priya and Hait, 2019). The details of TCLP, WET, and SPLP protocols are reported in supporting information.

### 2.3.3. ANC test

Expose of waste to acid rain, acidic surface, or groundwater, degradation of organic matter, or reactions of solid waste with atmospheric $CO_2$ leads to release of their toxic metals. Therefore, it is essential to determine the waste's ability to resist the acidic attack (Chen et al., 2009). The leaching test of ANC can be employed to obtain information about the hydration progression, immobilization performance in acidic environmental conditions, and the buffering capacity of waste against acidic attack (Bahaloo-Horeh et al., 2016). As pH decreases, the higher solubility of most of the metals occurs. Thus, a higher ANC means a higher resistance of waste against leaching in acidic conditions and confirms the chemical fixation of metals. Besides, the ANC test can identify the waste sensibility to small changes in pH (Buj et al., 2010).

ANC is determined by measuring the number of protons needed to change the initial pH of waste to a different pH value. This test consists of batch extraction series with increasing acid addition. In this way, various amounts of $HNO_3$ (1.0 M) was added to flasks containing SACCs powder (1 g) and deionized water (100 mL). The mixture was agitated for 24 h (until the pH value was constant); then, the pH values were measured. The titration curve was plotted based on measured pH values vs. the number of consumed protons (Bahaloo-Horeh et al., 2016).

### 2.3.4. Water washing

The water washing can eliminate most of the water-soluble salts, chlorides, and the amphoteric metals, for instance, Zn and Pb (due to their water solubility). For more information, the water solubility of metals presented in SACCs is listed in Table S1. These elements can contaminate the groundwater and soil if waste is inappropriately disposed of (Yan et al., 2018). In this regard, the SACCs powder was washed with deionized water in four washing steps at an L/S ratio of 20:1 and 60 °C for 1 h under agitation speed of 160 rpm. In each step, the liquid and solid residue were separated using a centrifuge. Then, the supernatant was collected for later analysis. Finally, the mix of four obtained supernatants was analyzed for metals concentration.

## 3. Results and discussion

### 3.1. Chemical composition of SACCs powder

Table S2 and Table 2 represent the chemical composition of the SACCs powder by XRF and acid digestion followed by ICP-MS,

**Table 1**
Calculation and classification of CF, GFC, and RAC indexes.

| Index | Formula | Limit value | Classification |
|---|---|---|---|
| CF | $CF = \frac{\text{Fraction 1} + \text{Fraction 2} + \text{Fraction 3}}{\text{Fraction 4}}$ | $CF < 1$ | Low contamination |
| | | $1 < CF < 3$ | Moderate contamination |
| | | $3 < CF < 6$ | Considerable contamination |
| | | $6 < CF$ | High contamination |
| GCF | $GCF = \sum CF$ | $GCF < 8$ | Low contamination |
| | | $8 < GCF < 16$ | Moderate contamination |
| | | $16 < GCF < 32$ | Considerable contamination |
| | | $32 < GCF$ | High contamination |
| RAC | $RAC = \frac{\text{Fraction 1}}{\text{Total metal concentration}} \times 100\%$ | $RAC < 1$ | No risk |
| | | $1 < RAC < 10$ | Low risk |
| | | $11 < RAC < 30$ | Medium risk |
| | | $31 < RAC < 50$ | High risk |
| | | $50 < RAC$ | Very high risk |

**Table 2**
Total elemental composition of the SACCs powder (mg/kg) using chemical digestion.

| Li | Be | | | | | | | | | | | B | C | N | O |
|---|---|---|---|---|---|---|---|---|---|---|---|---|---|---|---|
| 17 | 2 | | | | | | | | | | | n.a. | n.a. | n.a. | n.a. |
| Na | Mg | | | | | | | | | | | Al | Si | P | S |
| 1620 | 58400 | | | | | | | | | | | 204400 | 149800 | 10700 | 314 |
| K | Ca | Sc | Ti | V | Cr | Mn | Fe | Co | Ni | Cu | Zn | Ga | Ge | As | Se |
| 765 | 5918 | 22.5 | 2299 | 50 | 74 | 7504 | 6300 | 10.5 | 63 | 189 | 4500 | n.a. | n.a. | 377 | 1.3 |
| Rb | Sr | Y | Zr | Nb | Mo | Tc | Ru | Rh | Pd | Ag | Cd | In | Sn | Sb | Te |
| <1 | 2002 | 8.3 | 42057 | 40.1 | 31.4 | n.a. | n.a. | 250 | 4650 | 82.4 | <0.1 | <0.5 | 30.8 | 1.7 | 5.2 |
| Cs | Ba | La | Hf | Ta | W | Re | Os | Ir | Pt | Au | Hg | Tl | Pb | Bi | Po |
| <0.5 | 10100 | 4186 | 591 | 1.8 | 8.2 | n.a. | n.a. | n.a. | 75 | 5 | n.a. | <0.1 | 52 | 0.2 | n.a. |

| Lanthanides | Ce | Pr | Nd | Pm | Sm | Eu | Gd | Tb | Dy | Ho | Er | Tm | Yb | Lu |
|---|---|---|---|---|---|---|---|---|---|---|---|---|---|---|
| | 33195 | 1103 | 3429 | n.a. | 6.4 | 1.9 | 134 | 4.8 | 18.4 | n.a. | 4.9 | <0.1 | 4.7 | 0.3 |
| Actinides | Th | Pa | U | Np | Pu | Am | Cm | Bk | Cf | Es | Fm | Md | No | Lr |
| | 7.3 | n.a. | 1.5 | n.a. | n.a. | n.a. | n.a. | n.a. | n.a. | n.a. | n.a. | n.a. | n.a. | n.a. |

n.a.: not analyzed by ICP

respectively. The XRF analysis confirmed the results of ICP analysis. However, XRF cannot detect the elements with low concentration. According to the results of ICP-MS, the sum of the 61 elements in the SACCs powder accounted for 55.54 % of the total. The powder contained 20.44 wt% Al which was the most abundant element in SACCs powder. It makes the SACCs as a potential alternative resource in alumina production instead of bauxite ores. Silicon (14.98 wt%) was the second most concentrated compound. Other metals with significant amounts were Mg, Zr, Ce, P, Ba, Na, Mn, Fe, Zn, Ca, La, Pd, Nd, Ti, Sr, and Pr. The concentration of other metals was less than 1000 mg/kg.

One of the reasons for the deactivation of autocatalysts is facing chemical contaminants during their operational life. High temperatures cause catalyst module is melted with metals, such as Cu, Pb, Cr, Zn, Ni, Mg, Ca, P, and Fe, from lubricating oil, fuel gases, as well as the degradation and operation of the automobile engine, exhaust system, and converter canister (Coufalík et al., 2019). The presence of the mentioned contaminants was detected in SACCs powder used in this study, which is represented in Table S2 and Table 2.

The total level of REEs was approximately 4.21 wt%. Cerium was the most abundant REE presented in SACCs powder, followed by La, Nd, Pr, and Gd. The reported total REEs concentration in other sources is lower than SACCs. For example, the red mud contains 0.26 wt% REEs (Qu et al., 2019), and FCC-SC contains 1.5 wt% REEs (Thompson et al., 2017). It renders SACCs a suitable source of REEs to meet future demands.

The catalytic substances in SACCs used in this study were a combination of Pd, Rh, and Pt. Generally, the PGMs concentration in SACCs depends on catalytic converter construction, when it was manufactured, its application, the type of automobile, and the manufacturer (Fornalczyk and Saternus, 2013). The total concentrations of PGMs in SACCs used in this study were approximately 4975 mg/kg. In comparison, the PGMs content in proterozoic platinum ores and copper-nickel sulfide ores containing PGMs is about 1–10 mg/kg and 0.1–1 mg/kg, respectively (Chen and Huang, 2006). Thus, the SACCs can be considered as secondary rich sources of PGMs.

The results of the chemical composition of the SACCs powder used in this work are consistent with the literature. The typical main elements loading in SACCs used in different studies are shown in Table S3. To the best of our knowledge, the present study is the first report that has quantified or detected such a wide range of metals in SACCs.

### 3.2. CHNS analysis of SACCs powder

The results of CHNS analysis showed that the content of C, H, N, and S in SACCs powder was 3.24, 0.61, 1.74, and 1.10 wt%, respectively. Sulfur, carbon, and hydrocarbons are the contaminants that deposit on the surface of autocatalysts. It was reported that thermal treatment is needed for the catalysts with considerable contaminations to lower the carbon amounts (Mouna and Baral, 2019).

### 3.3. Element distribution of the SACCs powder

Fig. S1 shows the BSE image (Fig. S1(a)) and EDX-mapping analysis (Fig. S1(b)) to verify the presence of elements and trace out their arrangements and distribution in the powder. As seen, the aluminosilicate and aluminum oxide compounds were concentrated in the dark gray region in the BSE image, and different metal oxides load on them. According to Fig. S1(a) and (c), the PGMs and REEs content were more concentrated in the brighter regions.

As seen, the scattered pattern of elements indicates their uniform distribution. Besides, the results showed that the most element content in SACCs powder was oxygen (41.96 wt%), which is owing to the presence of metals, mainly in the oxide form.

### 3.4. Phase determination of SACCs powder

The XRD pattern of the SACCs powder is depicted in Table 3 and

**Table 3**
Crystallographic parameters of the different phases of the SACCs powder.

| Phase | Chemical formula | Content (wt%) | Space group |
|---|---|---|---|
| Indialite, syn | $Mg_2Al_4Si_5O_{18}$ | 82.9 | Hexagonal |
| Bjarebyite | $Ba(Mn,Fe)_2Al_2(PO_4)_3(OH)_3$ | 9.2 | Monoclinic |
| Baddeleyite, syn | $ZrO_2$ | 4.4 | Monoclinic |
| Monazite-(Ce), syn | $CePO_4$ | 3.5 | Monoclinic |

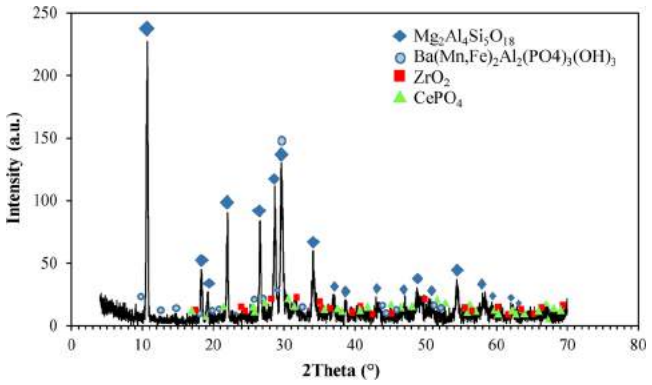


**Fig. 4.** XRD analysis of SACCs powder.

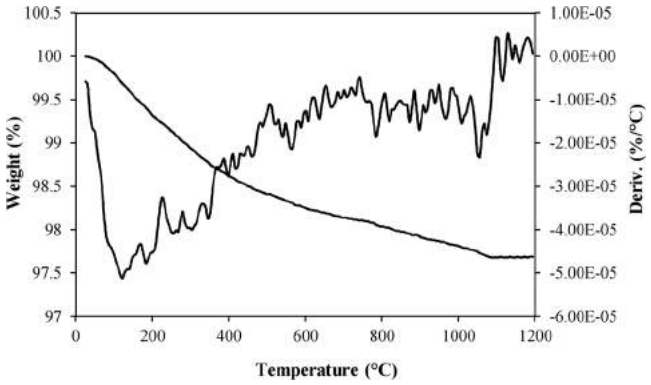


**Fig. 5.** TGA of the SACCs powder.

Fig. 4. The crystalline phases of $Mg_2Al_4Si_5O_{18}$, Ba $(Mn,Fe)_2Al_2(PO_4)_3(OH)_3$, $ZrO_2$, and $CePO_4$ were detected. The phases with low content cannot be identified by XRD analysis. The phases containing the metals of Al, Si, Mg, Zr, Ce, Ba, P, Mn, and Fe that had a concentration higher than 0.6 wt% (Table S2), were detected in XRD diffraction pattern.

As can be seen, the components were in oxide and phosphate form. Based on the XRD pattern, the cerium was in phosphate form. Other REEs were not detected, so it is not clear what phase they were in, maybe in oxide, hydroxide, or phosphate form. It was reported that the phosphate form is just found in vehicle-aged catalysts, not in new catalysts. Phosphorus is one of the catalyst contamination, which mainly originated from lubricating oils. More phosphorus concentrations than other contaminants cause a higher interaction probability of automotive catalyst components such as cerium oxide and aluminum oxide with phosphorus. It was reported that phosphorus could be found as aluminum, zirconium, cerium, calcium, and titanium phosphates in vehicle-aged catalysts (Kröger, 2007). Furthermore, the REEs tend to concentrate on aluminum phosphates such as $AlPO_4.2H_2O$ and $CaAl_3(PO_4)_2(OH)_5.H_2O$. A high affinity of lanthanum with phosphate was also reported (Li et al., 2018).

Another point is that the Si/Al ratio of $Mg_2Al_4Si_5O_{18}$ is 1.25, which shows that the autocatalyst is made of zeolite X. The Si/Al ratio in the range from 1 to 1.5 represents X-type zeolite with general formula of $(Li, Na, K)_p(Mg, Ca, Sr, Ba)_q[Al_{(p+2q)}Si_{n-(p+2q)}O_{2n}].m_0H_2O$, where $m_0$ is the water molecules number, q is the divalent metal ions number, p is the monovalent metal ion number, and n is the half of the oxygen atom number (Jha and Singh, 2011).

### 3.5. FTIR analysis of SACCs powder

The FTIR spectra of the SACCs were shown in Fig. S2. As observed, the peak at 3422.07 $cm^{-1}$ is related to the bending vibrations of O—H related to free water or interlayer adsorbed $H_2O$; it may be also due to the hydroxyl groups in Pt—OH structure (Ahmed et al., 2011). The peak at 1634.64 $cm^{-1}$ is related to the O—H bonds in aluminosilicate structure (Kalkan et al., 2013); also, the mentioned peak may be related to the aromatics and olefin adsorption on the surface of the catalyst. This may demonstrate that the coke species found near the active metal are soft coke, and it is mainly made up of heavy aromatics and unsaturated hydrocarbon (Ahmed et al., 2011). Although the presence of poison compounds such as coke could not be detected with XRD analysis, the presence of hydrocarbons was detected in FTIR peaks of SACCs. The peak at 1181.94 $cm^{-1}$ is associated with the asymmetric stretch of the Si-O, and the peak at 958.26 $cm^{-1}$ is caused by the Si(Al)-O stretching vibrations, which is sensitive to the Al and Si content (Kalkan et al., 2013). The peak at 909 $cm^{-1}$ is related to the asymmetric stretching vibration of Si-O-M (M = Si or Al) (Ndjock et al., 2017). Also, the peak at 578 $cm^{-1}$ is due to the deformation mode of the $PO_3$ group in the cerium phosphate structure (Masui et al., 2003). The peaks at 614.89 and 675.85 $cm^{-1}$ correspond to the stretch of the Al-O. The peak at 483.4 and 448 $cm^{-1}$ could be ascribed to the asymmetric stretching vibration of a metal oxide such as Fe-O, Si-O-Si, and $ZrO_2$ (wen Zhao et al., 2017; Khatri et al., 2010). As can be seen, the FTIR results confirmed the results of XRD, which shows that the metals are in oxide and phosphate form.

### 3.6. Thermal analysis of the SACCs powder

To investigate the correlation between temperature and weight changes, the thermal gravimetric analysis of the SACCs powder was conducted, and the result is shown in Fig. 5. With the temperature rise from 25 to 1200 °C, the weight loss of the powder took place at a relatively low rate. As a result, it had only 2.3 % weight loss. The low weight loss suggests that SACCs include low volatiles and contamination, such as carbon and sulfur. At the temperature > 1000 °C, no significant weight loss was observed. Generally, the SACCs powder is nearly stable up to 1000 °C, since no apparent decomposition behavior was observed. These results are the same as predicted because the autocatalysts have been worked in a high-temperature environment where unstable thermochemical materials cannot be selected.

The initial weight loss region up to 200 °C was due to the evaporation of water and the removal of volatile materials. The coke removal would not occur at this temperature region (Ahmed et al., 2011). Coke removal was taken place in several temperature regions (Sahoo et al., 2004). The weight loss between 200—400 °C may be due to the removal of soft coke (hydrogen-rich deposits forming from olefinic and/or paraffinic feedstocks) and the weight loss between 400—800 °C could be associated with the removal of hard coke or black coke (strongly hydrogen-deficient polynuclear aromatic deposits). The weight loss at temperatures near 800 °C or above may be related to the removal of hydrogen-free deposits (such as graphite) produced in catalytic reactions. Also, it was reported that sulfur removal occurs at a temperature of around 350—360 °C (Sahoo et al., 2004; Albers et al., 2008). As can be seen in TGA/DTA curves, there is a minimal increment in the sample weight, which is maybe due to the oxidation reactions such as the formation of PtO and PdO.

### 3.7. Surface morphology, particle size distribution and BET specific surface area

The wettability test results indicated that the SACCs powder had a hydrophilic surface with a contact angle of 41.17° and will be easily dispersed in water.

The microphotographs of the SACCs powder are illustrated in Fig. S3. The morphological structure of SACCs powder exhibited an irregular surface with a porous structure. Different particles have various texture, sizes, and shapes caused by various tensile and shearing forces

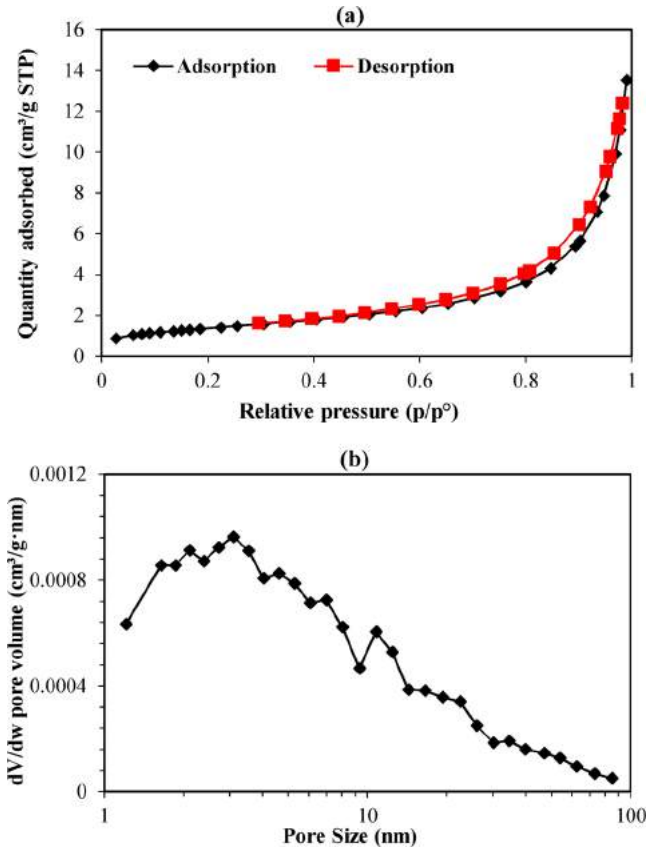


**Fig. 6.** (a) Nitrogen adsorption/desorption isotherms and (b) BJH model pore size distribution.

in the milling process of SACCs powder.

Shape and particle size are the two significant parameters that specify the surface area of the particles. A smaller particle size would obtain faster leaching kinetics since smaller particles provide the larger surface area in comparison with bigger particles (Rivera et al., 2019). Larger surface area causes full contact and reaction between particles and leaching reagents. While there would be a tendency for a very fine particle size of powder to aggregate, thus, the contact surface area is reduced, which leads to a reduction in the leaching efficiency (Zhao et al., 2019a).

The powder in this study had fine particles with a real density of 3.25 g/cm$^3$. The particle size distribution of the SACCs powder after crushing and milling is shown in Fig. S4. Based on the results, 100 % of particles were finer than 87 μm; the volume median diameter was 9.23 μm; $X_{10}$, $X_{50}$, and $X_{90}$ were 0.85, 3.67, and 24.94 μm, respectively, which shows a satisfactory result in comparison with the grinding effort ($X_{10}$, $X_{50}$, and $X_{90}$ show that the diameters of 10, 50 and 90 % of the particles, respectively, were below the mentioned values).

Fig. 6(a) shows the nitrogen adsorption-desorption isotherm of the SACCs powder at standard temperature and pressure (STP). Based on IUPAC recommendations, the shape of a gas adsorption isotherm of SACCs powder and hysteresis loop is related to Type IV and H3 classification, respectively. There is a turning point in the IV isotherm at the low relative pressure domain. However, a hysteresis loop was manifested in the high relative pressure region that can be ascribed to the capillary condensation phenomenon. The H3 hysteresis loop shows the presence of a mainly mesoporous structure in the SACCs powder. Isotherms with Type H3 loops were reported for components containing aggregates of particles with plate-like morphology, which leads to the formation of slit-like pores (Kruk and Jaroniec, 2001). The obtained results show that the average pore size diameter for the SACCs powder was 16.696 nm. Based on the IUPAC classification, the pore size between 2 and 50 nm is related to mesopores (Hosseini et al., 2018); thus, it could be concluded that the SACCs powder was mesoporous. Besides, as seen in the Barrett-Joyner-Halenda (BJH) model pore size distribution (Fig. 6(b)), there are mesopore peaks in the curve. It was shown that the diffusion in mesoporous is faster than micropore materials (Hu et al., 2019). The BET surface area for the SACCs powder was 5.0186 m$^2$/g. It has been found that the higher surface area of particles corresponds to higher leaching recovery. As mentioned earlier, there would be a tendency for a very fine particle size of powder to aggregate; thus, the contact surface area is reduced, leading to a reduction in the leaching efficiency (Zhao et al., 2019a).

### 3.8. Determination of initial pH and isoelectric point

The initial pH of the SACCs powder in deionized water was 7.8 after 24 h. This alkaline nature may be due to the presence of alkali metals, such as Na, Ba, Mg, Ca, and K, or an amphoteric effect of metal oxide compounds in the SACCs powder (Hopfe et al., 2018).

The zeta potential of the SACCs powder was defined as a function of pH at a fixed ionic strength of 0.01 M NaCl, and the results are shown in Fig. 7. As seen, the zeta potential of the powder depends on the pH because of the variation in the amount of deprotonation/protonation with different pH values. The zeta potential is negative at higher pH values, goes through zero, and becomes positive as the pH decreases. The negative zeta potential indicates that the net charge of a particle around its diffuse layer is negative, and the positive zeta potential shows a positively charged particle (Valix et al., 2001a). At the IEP, the number of negative sites is equal to the number of positive sites, and thus, there is no net charge on the particle surface. According to Fig. 7, the IEP of the SACCs powder occurs at pH 5.41. At pH values below the IEP, the surface of particle adsorbs more protons than hydroxyls, which resulted in the overall net positive charge on the surface. This phenomenon elevates easier access of anions (e.g., citrate and sulfate) to binding sites with a positive charge, which improves the leaching yield (Valix et al., 2001b).

### 3.9. Metals binding forms in SACCs powder

The distribution profile of metals at all the binding fractions is shown in Fig. 8 and Table 4. As seen, the metals binding fractions of powder were different from each other, and they distributed in all four steps of the sequential extraction; however, all of them were mainly exist in the residual fraction. Based on the BCR procedure, the residual fraction shows the existence of metals with a high stable binding structure. Under natural environmental conditions, the release of metals associated with the residual fraction is complicated, and only very severe and prolonged acidic conditions can mobilize them (Soliman et al., 2018). Barely mobile metals cause lower environmental impacts than easily mobile fractions. In the SACCs powder, the metals related to the residual fraction are probably to be accommodated in a stable form of aluminosilicate compounds. For example, the existence of Al in the residual fraction implies the extremely low mobilization of Al, which can be related to its dominant existence as a stable oxide ($Al_2O_3$) (Pathak et al., 2018). The presence of metals in residual fractions is following other studies showing that such metals are associated with Al-Si-oxides phases and/or embedded in glassy phases (Lin et al., 2018). Besides, some components (e.g., REEs) were in phosphate form, which had low solubility; thus, mobilization will only occur under strongly acidic conditions (Mittermüller et al., 2016).

In addition to mainly being present in the residual fraction, Al, Si, P, Ce, La, Nd, Pr, Mg, Pt, Pd, Fe, As, and Cr were found more in the reducible fraction. Among the metals associated with reducible fraction, aluminum had the most concentration (10,752 mg/kg). The oxidizable fraction of the SACCs was the smallest one. The presented metals in this fraction are related to the sulfides and organic matter. It indicates that under oxidizing conditions, part of these metals may be mobilized from

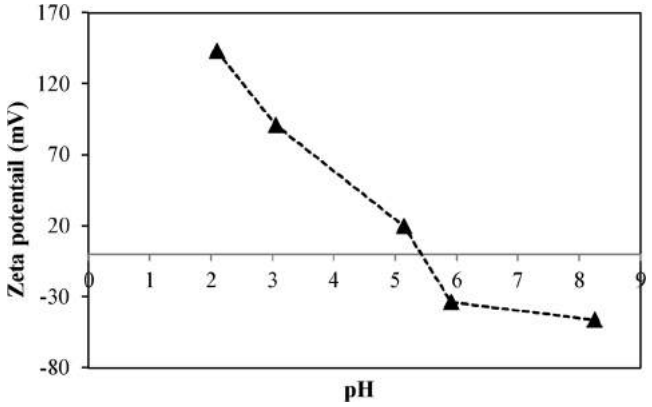


**Fig. 7.** The zeta potential of SACCs powder as a function of pH.

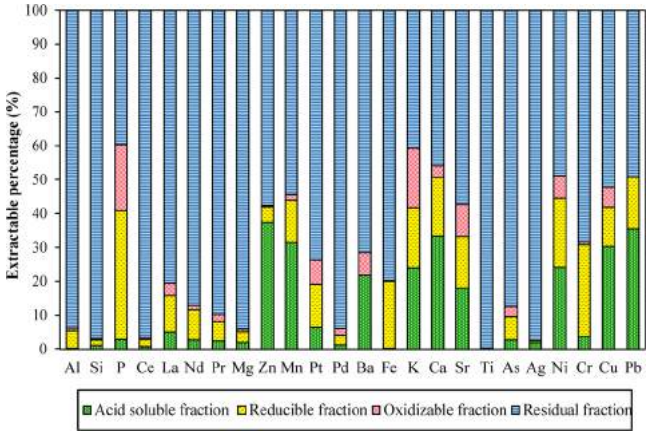


**Fig. 8.** Elements distribution for SACCs powder using the modified BCR procedure.

the SACCs (Pathak et al., 2018). Among the elements associated with oxidizable fraction, phosphorus had the most concentration (2099 mg/kg).

As said, in addition to mainly being present in the residual fraction, the amount of Zn, Mn, Ba, K, Ca, Sr, Ni, Cu, and Pb were found more in the acid-soluble fraction which indicated that the possible mobility of these metals is high. Among the metals associated with acid-soluble fraction, Mn had the most concentration (2360 mg/kg). Based on the BCR procedure, the variation in the pH and surrounding ionic composition easily affects the metals in the exchangeable fraction. The weak electrostatic attraction causes the weekly adsorption of these metals on the surface (Zhao et al., 2019b). This fraction exhibits the highest metal mobility and bioavailability; hence it is dangerous for the environment. Also, depending on the redox conditions, the reducible and oxidizable fraction may be a threat to the environment. The sum of the acid-soluble, reducible, and oxidizable fractions shows the total metal content related to the mobile phase (Dai et al., 2018). The high concentration of metals associated with the mobile phases represents that these metals may be easily mobilized by natural processes such as weathering, rainwater, microbial activities, and low molecular weight organic acids exudation by plant roots, which cause the transfer of metals into the food chain (Dai et al., 2018; Mittermüller et al., 2016).

### 3.9.1. Environmental implications

Table 4 shows the calculated CF, GCF, and RAC values for each metal of SACCs powder. Higher CF, GCF, and RAC values represent lower metal retention time, and higher metals treat to the environment. According to Table 4, most of the elements in SACCs powder had CF < 1 and thus posed a low degree of contamination. Some metals

**Table 4**
The element value based on modified BCR protocol and CF, GCF, and RAC indexes.

| | Al | Si | P | Ce | La | Nd | Pr | Mg | Zn | Mn | Pt | Pd | Ba | Fe | K | Ca | Sr | Ti | As | Ag | Ni | Cr | Cu | Pb | Sum |
|---|---|---|---|---|---|---|---|---|---|---|---|---|---|---|---|---|---|---|---|---|---|---|---|---|---|
| Fraction 1 (mg/kg) | 460 | 1592 | 296 | 259 | 211 | 92 | 26 | 1144 | 1688 | 2360 | 5 | 55 | 2192 | 11 | 183 | 1976 | 363 | 2 | 10 | 2 | 15 | 3 | 57 | 18 | 13,020 |
| Fraction 2 (mg/kg) | 10,752 | 2460 | 4072 | 676 | 452 | 306 | 63 | 1884 | 202 | 936 | 10 | 139 | 8 | 1248 | 136 | 1016 | 302 | 2 | 26 | 0 | 13 | 20 | 22 | 8 | 24,754 |
| Fraction 3 (mg/kg) | 1627 | 431 | 2099 | 166 | 151 | 43 | 23 | 393 | 17 | 121 | 5 | 91 | 678 | 6 | 134 | 206 | 190 | 0 | 11 | 0 | 4 | 1 | 11 | 0 | 6408 |
| Fraction 4 (mg/kg) | 191,561 | 145,317 | 4233 | 32,094 | 3372 | 2988 | 991 | 54,979 | 2593 | 4087 | 55 | 4365 | 7221 | 5035 | 312 | 2720 | 1147 | 2295 | 330 | 80 | 31 | 51 | 99 | 26 | 465,981 |
| Σ(F1 + F2 + F3) (mg/kg) | 12,839 | 4483 | 6467 | 1101 | 814 | 441 | 112 | 3421 | 1907 | 3417 | 20 | 285 | 2879 | 1265 | 453 | 3198 | 855 | 4 | 47 | 2 | 32 | 23 | 90 | 26 | 44,183 |
| CF | 0.07 | 0.03 | 1.53 | 0.03 | 0.24 | 0.15 | 0.11 | 0.06 | 0.74 | 0.84 | 0.36 | 0.07 | 0.40 | 0.25 | 1.45 | 1.18 | 0.75 | 0.00 | 0.14 | 0.02 | 1.05 | 0.46 | 0.92 | 1.03 | 11.87 (≈CFG) |
| RAC (%) | 0.23 | 1.06 | 2.77 | 0.78 | 5.05 | 2.67 | 2.36 | 1.96 | 37.51 | 31.45 | 6.40 | 1.19 | 21.70 | 0.18 | 23.95 | 33.39 | 18.12 | 0.09 | 2.65 | 1.94 | 24.13 | 3.78 | 30.26 | 35.38 | – |

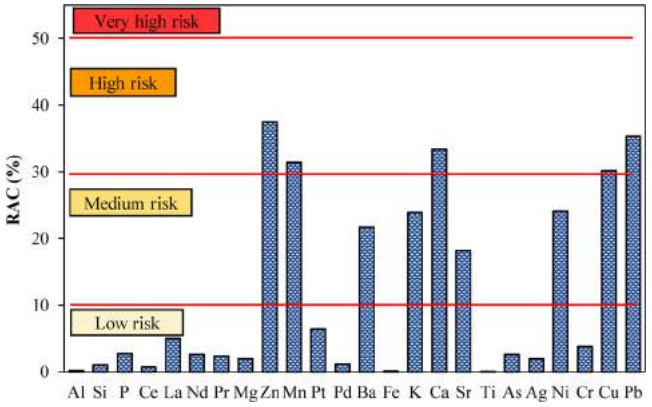


**Fig. 9.** The comparison of RAC values for metals of SACCs powder.

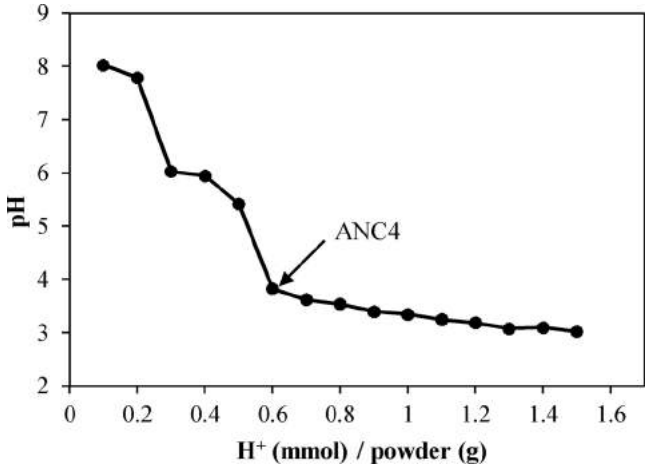


**Fig. 10.** The ANC of the SACCs powder.

such as Ni and Pb had $1 < CF < 3$ and fell in the moderate contamination category. The GCF index is equal to the sum of the CF indexes of all the elements. Based on Table 4, the value of GCF was 11.87, which depicts SACCs have a moderate degree of contamination. Fig. 9 shows the comparison of RAC values for metals of SACCs. It can be seen that Zn, Mn, Ca, Cu, and Pb posed a high risk due to their high RAC values. The metals of Ba, Sr, and Ni in SACCs fell in the medium-risk category. Besides, the other metals (Si, La, Nd, Pr, Mg, Pt, Pd, As, and Cr) were at low environmental risk. Base on RAC grade, the Al, Fe, Ce, and Ti came under no environmental risk rank. Also, there were no metals at very high-risk classification.

It is worth noting that despite the small calculated index of CF and RAC for some metals, which is a signature of low contamination degree, the total amount of metals mobilization was high ($\Sigma(F1+F2+F3)$) and causes serious hazards. Indeed, contamination indexes evaluate the content of mobilized metal concerning the residual fraction or total metal concentration of waste. Nevertheless, the total metal content presented in the SACCs was very high.

### 3.10. Leaching assessment tests

#### 3.10.1. Determination of ANC

The ANC of the SACCs powder is presented in Fig. 10. The ANC is calculated from the acidity to change the initial pH of waste to a reference pH value, which is called "$ANC_X$" (the selected reference pH defines the subindex of ANC). For the SACCs powder, the pH value was reduced rapidly by the addition of acid. After the addition of 0.6 mmol $H^+$/g SACCs powder, the final pH value reached 4 ($ANC_4$). The pH value changes were more gradual from pH 4 to the final pH of 3, and more acid was required to reach pH 3. The $ANC_3$ of powder was 1.5 mmol $H^+$/g SACCs powder. It means when the final pH reached 3, 1.5 mmol $H^+$ by 1 g of powder was consumed. Finally, it could be concluded that the pH of the SACCs powder reduced simply in contact with acid, and acid neutralization capacity of waste was low.

#### 3.10.2. TCLP, WET, and SPLP tests

The results of TCLP, SPLP, and WET with their threshold limits based on the California Department of Toxic Substances Control (CDTSC) and the United States Environmental Protection Agency (USEPA) are shown in Table 5. Although there are no standard limits for some metals in USEPA and CDTSC regulatory levels, the extraction results of all metals presented in the SACCs powder were also reported. As seen, among the leaching tests, the WET was the most aggressive procedure to assess mobility. It is due to this fact that citrate, which is a trident ligand, can cause the metal chelates formation in solution. The complexes/ion pairs with mono-dentated ligands (such as acetate complexes) are less stable than metal chelates with trident ligands (González and Barnes, 2002). As expected, all metals (except Mg) had the greatest affinity with citrate ligand among three performed leaching tests.

In comparison between TCLP and SPLP, all metals had a higher concentration in TCLP leachates (except Ba), which is ascribed to the difference of extraction ability of acetic acid buffer solution and unbuffered nitric acid-sulfuric acid solution. It demonstrates their susceptibility to the acidic landfill condition and their tendency to leach when compared to acidic rain conditions (Priya and Hait, 2019). Ba concentration in leachates of SPLP was higher than the TCLP test, representing the higher leaching potential of nitric acid-sulfuric acid than acetic acid. Indeed, the leaching system's chemical essence, the dependency of metals towards the leaching ions, and the competitive situation for the redox reaction in the solution affect the order of leached metals.

To pass the leaching tests, the leached metals concentration should be less than the standard limits in USEPA and CDTSC regulatory levels. The results showed all elements in the SACCs, which USEPA and CDTSC have determined their standard limits, passed the WET, SPLP, and TCLP tests and remained within the regulatory limits, but Ba exceeded the regulatory limit according to WET. The SACCs included 10,100 mg/kg Ba and failed the 100 mg/L WET Ba standard by generating a solution

**Table 5**
Leaching concentration of metals (mg/L) from SACCs, according to TCLP, SPLP, and WET.

| Metal | TCLP | TCLP limit | SPLP | SPLP limit | WET | SPLP limit |
|---|---|---|---|---|---|---|
| Al | 1.78 | n.s. | 0.21 | n.s. | 756.1 | n.s. |
| Si | 21.2 | n.s. | 0 | n.s. | 185.4 | n.s. |
| Ce | 2.62 | n.s. | 0.14 | n.s. | 256.1 | n.s. |
| La | 1.41 | n.s. | 0.27 | n.s. | 89.4 | n.s. |
| Nd | 0.65 | n.s. | 0.19 | n.s. | 40.9 | n.s. |
| Pr | 0.29 | n.s. | 0.24 | n.s. | 4.45 | n.s. |
| Mg | 243.4 | n.s. | 5.48 | n.s. | 188.6 | n.s. |
| Zn | 21.1 | n.s. | 0 | n.s. | 186.4 | 250 |
| Mn | 36.3 | n.s. | 0.26 | n.s. | 318.8 | n.s. |
| Pt | 0.28 | n.s. | 0.06 | n.s. | 0.5 | n.s. |
| Pd | 1.38 | n.s. | 0.07 | n.s. | 8.42 | n.s. |
| Ba | 3.81 | 100 | 5.86 | 100 | 347 | 100 |
| Fe | 11.4 | n.s. | 0.33 | n.s. | 60.3 | n.s. |
| Ca | 30 | n.s. | 4.36 | n.s. | 194.9 | n.s. |
| Sr | 7.62 | n.s. | 2.29 | n.s. | 48.6 | n.s. |
| Ti | 0 | n.s. | 0 | n.s. | 4.01 | n.s. |
| As | 0.11 | n.s. | 0.02 | n.s. | 2.63 | n.s. |
| Ag | 0 | 5 | 0 | n.s. | 0.16 | n.s. |
| Ni | 0.2 | n.s. | 0 | n.s. | 1.35 | 20 |
| Cr | 0.03 | 5 | 0 | 5 | 0.74 | 6;560 (Cr VI;III) |
| Cu | 0.11 | n.s. | 0 | n.s. | 3.35 | 25 |
| Pb | 0.02 | 5 | 0 | 5 | 0.91 | 5 |

n.s.: not stated.

**Table 6**
Removal of soluble elements from SACCs by water washing.

| Element | Cl | Na | K | P | Sr | Ca | Ba | As | Al | Mg | Zn | Mn |
|---|---|---|---|---|---|---|---|---|---|---|---|---|
| Removal (mg/L) | 28 | 18.40 | 2.29 | 2.91 | 0.53 | 0.89 | 1.25 | 0.03 | 9.84 | 1.38 | 0.09 | 0.11 |
| Removal efficiency (%) | n.d. | 94.27 | 24.85 | 2.26 | 2.20 | 1.25 | 1.03 | 0.66 | 0.40 | 0.20 | 0.17 | 0.12 |

n.d.: not determined.

**Table 7**
The potential economic value of metals contained in SACCs.

| Metal | Content (mg/kg SACCs) | Price ($US/kg) | Economic worth ($US/t SACCs) |
|---|---|---|---|
| Pd | 4650 | 72351.93 (www.metalary.com) | 336436.47 |
| Pt | 75 | 33025.20 (www.metalary.com) | 2476.89 |
| Rh | 250 | 302216.58 (www.metalary.com) | 75554.15 |
| Hf | 591 | 5926.03 (www.mineralprices.com) | 3502.28 |
| Zr | 42,057 | 37.13 (https://institut-seltene-erden.de/) | 1561.58 |
| Al | 204,400 | 1.77 (www.metalary.com) | 361.79 |
| Sr | 2002 | 100 (www.alibaba.com) | 200.2 |
| Nd | 3429 | 52.86 (https://institut-seltene-erden.de/) | 181.26 |
| Ce | 33195 | 4.71 (https://institut-seltene-erden.de/) | 156.35 |
| Ti | 2299 | 58.09 (www.mineralprices.com) | 133.55 |
| Pr | 1103 | 95.01 (https://institut-seltene-erden.de/) | 104.79 |
| La | 4186 | 4.93 (https://institut-seltene-erden.de/) | 20.64 |
| Mn | 7504 | 2.06 (www.metalary.com) | 15.46 |
| Zn | 4500 | 2.27 (www.metalary.com) | 10.22 |
| Fe | 6300 | 0.09 (www.metalary.com) | 0.57 |
| Sum | | | 420716.2 |

with 347 mg/L Ba.

As said before, there is no standard threshold for some metals in USEPA and CDTSC regulatory levels. The results showed that the concentration of these metals under different leaching tests were also high. It is worthy to note that all metals are toxic at elevated concentrations (Dopson et al., 2014). Therefore, this waste should be disposed of safely.

#### *3.10.3. Effect of water washing*

The content of soluble elements in the washing water is shown in Table 6. As observed, the removal of some elements, such as Cl and Na, was significant. The elements, including P, Ca, Ba, and Sr, were partially dissolved. It can be included that open area storage of the SACCs may cause environmental leachate problems due to water leaching of mentioned metals. However, since the dissolution of other metals was negligible, the water washing pretreatment before the leaching process can be done to leach the soluble salts. This pretreatment leads to a decrease in acid consumption in the leaching process (alkali salts consume large amounts of acid). Also, evaporation of the alkaline water solution can cause obtaining the alkaline salt. In the alkaline leaching process, the water washing pretreatment should be disregarded since it allows applying lower alkaline reagent (Sadeghi et al., 2017).

## 4. SACCs: an asset or a liability

SACCs can be considered as secondary metal resources for rare earth metals like Ce, La, Nd, Pr, Dy, and precious metals such as Pt, Pd, Rh, and metals with an industrial application, such as Al, Zn, Mn, Zn, Fe, Ti, and Sr. Indeed, SACCs can assist in fulfilling the needs of metals. Table 7 shows the economic value of several metals contained in SACCs (based on the metal content of the present study). It can be seen that there is a great potential wealth in SACCs.

Considering the tremendous amount of produced SACCs and their high metal content, they should be regarded as an asset. On the other hand, the metals presented in the SACCs can contaminate the soil, water, and air and pose environmental impacts on natural resources and humankind. These adverse effects lead the SACCs to the liability category. Nonetheless, the metals can be retrieved by proper recycling that not only decreases the metal contamination problem but also enhances the life of non-renewable resources. Furthermore, correct regulations and policies should be formulated for proper collection and control of informal recycling. Consequently, the SACCs could qualify for the asset category.

## 5. Conclusions

This research comprehensively characterized SACCs from different aspects, which is extremely important for future studies involving the recycling processes. The study showed that SACCs are a very rich source of REEs (42,119 mg/kg) and PGMs (4975 mg/kg), compared to other secondary sources, which could give the SACCs real market value. It was concluded that SACCs must be recycled both from the economic and environmental points of view. The detailed information about the leaching behavior of metals through the toxicity tests of SPLP, TCLP, WET, as well as the calculation of CF, GCF, and RAC parameters, declared that the SACCs should be considered as hazardous waste regarding the high mobilization of toxic metals under different environmental conditions. However, based on the results of the modified BCR procedure, a unique harsh recycling approach is required due to the stable binding structure of SACCs, metals embedded in silicate phases, and the presence of barely soluble metal phosphates. The outcomes of the present work can be beneficial for enabling the development of appropriate recycling approaches.

## CRediT authorship contribution statement

**Nazanin Bahaloo-Horeh:** Investigation, Methodology, Formal analysis, Conceptualization, Writing - original draft, Writing - review & editing. **Seyyed Mohammad Mousavi:** Validation, Project administration, Funding acquisition, Supervision, Writing - review & editing.

## Declaration of Competing Interest

The authors declare that they have no known competing financial interests or personal relationships that could have appeared to influence the work reported in this paper.

## Acknowledgments

This study was financially supported by Tarbiat Modares University under grant number IG-39701. The authors also thank the Biotechnology Development Council of the Islamic Republic of Iran for their supports under grant number 970507.

## Appendix A. Supplementary data

Supplementary material related to this article can be found, in the online version, at doi:https://doi.org/10.1016/j.jhazmat.2020.123186.

## References

Ahmed, R., Sinnathambi, C.M., Subbarao, D., 2011. Kinetics of de-coking of spent reforming catalyst. J. Appl. Sci. 11, 1225–1230.
Albers, P.W., Weitkamp, J., Carbonaceous Deposits, Handb., 2008. Heterog. Catal. Online. 1197–1217.
Azevedo, D.M.F., Silva, J.A.S., Servulo, E.F.C., Frescura, V.L.A., Dognini, J., Oliveira, F.J.S., 2019. Recovery of lanthanides from hydrocarbon cracking spent catalyst through chemical and biotechnological strategies. J. Environ. Sci. Heal. Part A. 54, 686–693.
Bahaloo-Horeh, N., Mousavi, S.M., Shojaosadati, S.A., 2016. Bioleaching of valuable metals from spent lithium-ion mobile phone batteries using *Aspergillus niger*. J. Power Sources 320, 257–266.
Bahaloo-Horeh, N., Vakilchap, F., Mousavi, S.M., 2019. Bio-hydrometallurgical methods for recycling spent lithium-ion batteries. Recycl. Spent Lithium-Ion Batter. Springer, pp. 161–197.
Buj, I., Torras, J., Rovira, M., de Pablo, J., 2010. Leaching behaviour of magnesium phosphate cements containing high quantities of heavy metals. J. Hazard. Mater. 175, 789–794.
Cabral, M., Pedrosa, F., Margarido, F., Nogueira, C.A., 2013. End-of-life Zn–$MnO_2$ batteries: electrode materials characterization. Environ. Technol. 34, 1283–1295.
Chen, J., Huang, K., 2006. A new technique for extraction of platinum group metals by pressure cyanidation. Hydrometallurgy. 82, 164–171.
Chen, Q., Zhang, L., Ke, Y., Hills, C., Kang, Y., 2009. Influence of carbonation on the acid neutralization capacity of cements and cement-solidified/stabilized electroplating sludge. Chemosphere 74, 758–764.
Chen, A., Wang, S., Zhang, L., Peng, J., 2015. Optimization of the microwave roasting extraction of palladium and rhodium from spent automobile catalysts using response surface analysis. Int. J. Miner. Process. 143, 18–24.
Chen, Y., Chen, M., Li, Y., Wang, B., Chen, S., Xu, Z., 2018. Impact of technological innovation and regulation development on e-waste toxicity: a case study of waste mobile phones. Sci. Rep. 8, 7100.
Choi, I.-H., Kim, H.-R., Moon, G., Jyothi, R.K., Lee, J.-Y., 2018. Spent $V_2O_5$-$WO_3$/$TiO_2$ catalyst processing for valuable metals by soda roasting-water leaching. Hydrometallurgy. 175, 292–299.
Coufalík, P., Matoušek, T., Křůmal, K., Vojtíšek-Lom, M., Beránek, V., Mikuška, P., 2019. Content of metals in emissions from gasoline, diesel, and alternative mixed biofuels. Environ. Sci. Pollut. Res. 26, 29012–29019.
Dai, Z., Wang, L., Tang, H., Sun, Z., Liu, W., Sun, Y., et al., 2018. Speciation analysis and leaching behaviors of selected trace elements in spent SCR catalyst. Chemosphere. 207, 440–448.
de Andrade Passos, E., Alves, J.C., dos Santos, I.S., Jose do Patrocínio, H.A., Garcia, C.A.B., Costa, A.C.S., 2010. Assessment of trace metals contamination in estuarine sediments using a sequential extraction technique and principal component analysis. Microchem. J. 96, 50–57.
Dopson, M., Ossandon, F.J., Lövgren, L., Holmes, D.S., 2014. Metal resistance or tolerance? Acidophiles confront high metal loads via both abiotic and biotic mechanisms. Front. Microbiol. 5, 157.
ELTurk, M., Abdullah, R., Rozainah, M.Z., Bakar, N.K.A., 2018. Evaluation of heavy metals and environmental risk assessment in the Mangrove Forest of Kuala Selangor estuary, Malaysia. Mar. Pollut. Bull. 136, 1–9.
Firmansyah, M.L., Kubota, F., Goto, M., 2019. Selective recovery of platinum group metals from spent automotive catalysts by leaching and solvent extraction. J. Chem. Eng. JAPAN. 52, 835–842.
Fontana, D., Pietrantonio, M., Pucciarmati, S., Rao, C., Forte, F., 2019. A comprehensive characterization of End-of-Life mobile phones for secondary material resources identification. Waste Manag. 99, 22–30.
Fornalczyk, A., Saternus, M., 2013. Vapour treatment method against other pyro-and hydrometallurgical processes applied to recover platinum form used auto catalytic converters. Acta Metall. Sin. 26, 247–256.
Funari, V., Mäkinen, J., Salminen, J., Braga, R., Dinelli, E., Revitzer, H., 2017. Metal removal from Municipal Solid Waste Incineration fly ash: a comparison between chemical leaching and bioleaching. Waste Manag. 60, 397–406.
Gao, L., Wang, Z., Li, S., Chen, J., 2018. Bioavailability and toxicity of trace metals (Cd, Cr, Cu, Ni, and Zn) in sediment cores from the Shima river, South China. Chemosphere. 192, 31–42.
González, A.M., Barnes, R.M., 2002. Comparison of microwave-assisted extraction and waste extraction test (WET) preparation for inductively coupled plasma spectroscopic analyses of waste samples. Anal. Bioanal. Chem. 374, 255–261.
Gwebu, S., Tavengwa, N.T., Klink, M.J., Mtunzi, F.M., Modise, S.J., Pakade, V.E., 2017. Quantification of Cd, Cu, Pb and Zn from sewage sludge by modified-BCR and ultrasound assisted-modified BCR sequential extraction methods. African J. Pure Appl. Chem. 11.
Hira, M., Yadav, S., Morthekai, P., Linda, A., Kumar, S., Sharma, A., 2018. Mobile Phones—An asset or a liability: A study based on characterization and assessment of metals in waste mobile phone components using leaching tests. J. Hazard. Mater. 342, 29–40.
Hopfe, S., Konsulke, S., Barthen, R., Lehmann, F., Kutschke, S., Pollmann, K., 2018. Screening and selection of technologically applicable microorganisms for recovery of rare earth elements from fluorescent powder. Waste Manag. 79, 554–563.
Hosseini, H., Kokabi, M., Mousavi, S.M., 2018. BC/rGO conductive nanocomposite aerogel as a strain sensor. Polymer (Guildf). 137, 82–96.
Hu, H.-Y., Xie, N., Wang, C., Wu, F., Pan, M., Li, H.-F., et al., 2019. Enhancing the performance of motive power lead-acid batteries by high surface area carbon black additives. Appl. Sci. 9, 186.
Islam, K.M.N., Hildenbrand, J., Hossain, M.M., 2018. Life cycle impacts of three-way ceramic honeycomb catalytic converter in terms of disability adjusted life year. J. Clean. Prod. 182, 600–615.
ISO17892-part3, 2015. Geotechnical Investigation and Testing-laboratory Testing of Soil-part 3: Determination of Particle Density, (2015).
Jaishankar, M., Tseten, T., Anbalagan, N., Mathew, B.B., Beeregowda, K.N., 2014. Toxicity, mechanism and health effects of some heavy metals. Interdiscip. Toxicol. 7, 60–72.
Jha, B., Singh, D.N., 2011. A review on synthesis, characterization and industrial applications of flyash zeolites. J. Mater. Educ. 33, 65.
Kalavrouziotis, I.K., Koukoulakis, P.H., 2009. The environmental impact of the platinum group elements (Pt, Pd, Rh) emitted by the automobile catalyst converters. Water Air Soil Pollut. 196, 393.
Kalkan, E., Nadaroglu, H., Dikbas, N., Tasgin, E., Celebi, N., 2013. Bacteria-modified red mud for adsorption of cadmium ions from aqueous solutions. Pol J Env. Stud. 22, 105–117.
Karim, S., Ting, Y.-P., 2020. Ultrasound-assisted nitric acid pretreatment for enhanced biorecovery of platinum group metals from spent automotive catalyst. J. Clean. Prod., 120199.
Khatri, C., Mishra, M.K., Rani, A., 2010. Synthesis and characterization of fly ash supported sulfated zirconia catalyst for benzylation reactions. Fuel Process. Technol. 91, 1288–1295.
Kohl, C.A., Gomes, L.P., 2018. Physical and chemical characterization and recycling potential of desktop computer waste, without screen. J. Clean. Prod. 184, 1041–1051.
Kröger, V., 2007. Poisoning of automotive exhaust gas catalyst components: the role of phosphorus in the poisoning phenomena. University of Oulu.
Kruk, M., Jaroniec, M., 2001. Gas adsorption characterization of ordered organic− inorganic nanocomposite materials. Chem. Mater. 13, 3169–3183.
Kumar, A., Kuppusamy, V.K., Holuszko, M., Song, S., Loschiavo, A., 2019. LED lamps waste in Canada: generation and characterization. Resour. Conserv. Recycl. 146, 329–336.
Li, Z., Qiu, Z., Yang, J., Ma, B., Lu, S., Qin, C., 2018. Investigation of phosphate adsorption from an aqueous solution using spent fluid catalytic cracking catalyst containing lanthanum. Front. Environ. Sci. Eng. 12, 15.
Lin, R., Stuckman, M., Howard, B.H., Bank, T.L., Roth, E.A., Macala, M.K., et al., 2018. Application of sequential extraction and hydrothermal treatment for characterization and enrichment of rare earth elements from coal fly ash. Fuel. 232, 124–133.
Macías, F., Pérez-López, R., Caraballo, M.A., Cánovas, C.R., Nieto, J.M., 2017. Management strategies and valorization for waste sludge from active treatment of extremely metal-polluted acid mine drainage: a contribution for sustainable mining. J. Clean. Prod. 141, 1057–1066.
Malhotra, J., Bhandwal, M., Tyagi, R.K., Kalia, A., Pandey, S., Rahul, A., 2015. Ecofriendly catalytic converter to reduce biochemical effect of exhaust gases. Der Pharma Chem. 7, 56–61.
Masui, T., Hirai, H., Imanaka, N., Adachi, G., 2003. Characterization and thermal behavior of amorphous cerium phosphate. Phys. Status Solidi 198, 364–368.
Mittermüller, M., Saatz, J., Daus, B., 2016. A sequential extraction procedure to evaluate the mobilization behavior of rare earth elements in soils and tailings materials. Chemosphere. 147, 155–162.
Morcali, M.H., 2020. A new approach to recover platinum-group metals from spent catalytic converters via iron matte. Resour. Conserv. Recycl. 159, 104891.
Mouna, H.M., Baral, S.S., 2019. A bio-hydrometallurgical approach towards leaching of lanthanum from the spent fluid catalytic cracking catalyst using *Aspergillus niger*. Hydrometallurgy. 184, 175–182.
Naseri, T., Bahaloo-Horeh, N., Mousavi, S.M., 2019. Bacterial leaching as a green approach for typical metals recovery from end-of-life coin cells batteries. J. Clean. Prod. 220, 483–492.
Ndjock, B.I.D.L., Elimbi, A., Cyr, M., 2017. Rational utilization of volcanic ashes based on factors affecting their alkaline activation. J. Non. Solids 463, 31–39.
Nikfar, S., Parsa, A., Bahaloo-Horeh, N., Mousavi, S.M., 2020. Enhanced bioleaching of Cr and Ni from a chromium-rich electroplating sludge using the filtrated culture of *Aspergillus niger*. J. Clean. Prod., 121622.
Pathak, A., Healy, M.G., Morrison, L., 2018. Changes in the fractionation profile of Al, Ni, and Mo during bioleaching of spent hydroprocessing catalysts with *Acidithiobacillus ferrooxidans*. J. Environ. Sci. Heal. Part A. 53, 1006–1014.
Priya, A., Hait, S., 2019. Toxicity characterization of heavy metals from waste printed circuit boards. Waste Manag. Resour. Effic. Springer, pp. 833–840.
Qu, Y., Li, H., Wang, X., Tian, W., Shi, B., Yao, M., et al., 2019. Bioleaching of major, Rare Earth, and radioactive elements from red mud by using indigenous

chemoheterotrophic bacterium *Acetobacter* sp. Minerals. 9, 67.
Rebello, R.Z., Lima, M.T.W.D.C., Yamane, L.H., Siman, R.R., 2020. Characterization of end-of-life LED lamps for the recovery of precious metals and rare earth elements. Resour. Conserv. Recycl. 153, 104557.
Rivera, R.M., Ounoughene, G., Malfliet, A., Vind, J., Panias, D., Vassiliadou, V., et al., 2019. A Study of the occurrence of selected rare-earth elements in neutralized–leached bauxite residue and comparison with untreated bauxite residue. J. Sustain. Metall. 1–12.
Rzelewska, M., Regel-Rosocka, M., 2018. Wastes generated by automotive industry–Spent automotive catalysts. Phys. Sci. Rev. 3.
Sadeghabad, M.S., Bahaloo-Horeh, N., Mousavi, S.M., 2019. Using bacterial culture supernatant for extraction of manganese and zinc from waste alkaline button-cell batteries. Hydrometallurgy. 188, 81–91.
Sadeghi, S.M., Vanpeteghem, G., Neto, I.F.F., Soares, H.M.V.M., 2017. Selective leaching of Zn from spent alkaline batteries using environmentally friendly approaches. Waste Manag. 60, 696–705.
Sahoo, S.K., Ray, S.S., Singh, I.D., 2004. Structural characterization of coke on spent hydroprocessing catalysts used for processing of vacuum gas oils. Appl. Catal. A Gen. 278, 83–91.
Senthil, K., Akiba, U., Fujiwara, K., Hamada, F., Kondo, Y., 2017. High selectivity and extractability of palladium from chloride leach liquors of an automotive catalyst residue by azothiacalix [4] arene derivative. Hydrometallurgy. 169, 478–487.
Singh, N., Duan, H., Yin, F., Song, Q., Li, J., 2018. Characterizing the materials composition and recovery potential from waste mobile phones: a comparative evaluation of cellular and smart phones. ACS Sustain. Chem. Eng. 6, 13016–13024.
Soliman, N.F., El Zokm, G.M., Okbah, M.A., 2018. Risk assessment and chemical fractionation of selected elements in surface sediments from Lake Qarun, Egypt using modified BCR technique. Chemosphere. 191, 262–271.
Spooren, J., Atia, T.A., 2020. Combined microwave assisted roasting and leaching to recover platinum group metals from spent automotive catalysts. Miner. Eng. 146, 106153.
Thompson, V.S., Gupta, M., Jin, H., Vahidi, E., Yim, M., Jindra, M.A., et al., 2017. Techno-economic and life cycle analysis for bioleaching rare-earth elements from waste materials. ACS Sustain. Chem. Eng. 6, 1602–1609.
Valix, M., Usai, F., Malik, R., 2001a. The electro-sorption properties of nickel on laterite gangue leached with an organic chelating acid. Miner. Eng. 14, 205–215.
Valix, M., Tang, J.Y., Cheung, W.H., 2001b. The effects of mineralogy on the biological leaching of nickel laterite ores. Miner. Eng. 14, 1629–1635.
Voncken, J.H.L., 2019. Recovery of ce and la from spent automotive catalytic converters. Crit. Rare Earth Elem. Recover. from Second. Resour. 267.
Wang, L., He, J., Xia, A., Cheng, M., Yang, Q., Du, C., et al., 2017. Toxic effects of environmental rare earth elements on delayed outward potassium channels and their mechanisms from a microscopic perspective. Chemosphere 181, 690–698.
wen Zhao, Z., yuan Chai, L., Peng, B., jie Liang, Y., He, Y., hao Yan, Z., 2017. Arsenic vitrification by copper slag based glass: mechanism and stability studies. J. Non. Solids 466–467, 21–28.
Winslow, K.M., Laux, S.J., Townsend, T.G., 2018. A review on the growing concern and potential management strategies of waste lithium-ion batteries. Resour. Conserv. Recycl. 129, 263–277.
Xiang, Y., Yang, X., Xu, Z., Hu, W., Zhou, Y., Wan, Z., et al., 2020. Fabrication of sustainable manganese ferrite modified biochar from vinasse for enhanced adsorption of fluoroquinolone antibiotics: effects and mechanisms. Sci. Total Environ. 709, 136079.
Yan, D., Peng, Z., Yu, L., Sun, Y., Yong, R., Karstensen, K.H., 2018. Characterization of heavy metals and PCDD/Fs from water-washing pretreatment and a cement kiln co-processing municipal solid waste incinerator fly ash. Waste Manag. 76, 106–116.
Yeom, J.-M., Jung, H.-J., Choi, S.-Y., Lee, D.S., Lim, S.-R., 2018. Environmental effects of the technology transition from liquid-crystal display (LCD) to organic light-emitting diode (OLED) display from an E-Waste management perspective. Int. J. Environ. Res. 12, 479–488.
Zhao, Z., Qiu, Z., Yang, J., Ma, B., Li, Z., Lu, S., et al., 2019a. Recovery of rare earth element cerium from spent automotive exhaust catalysts using a novel method. Waste Biomass Valorization 1–10.
Zhao, K., Hu, Y., Wang, Y., Chen, D., Feng, Y., 2019b. Speciation and risk assessment of heavy metals in municipal solid waste incineration fly ash during thermal processing. Energy Fuels 33, 10066–10077.